



MemoryMamba: Memory-Augmented State Space Model for Defect Recognition

Qianning Wang¹, He Hu², Yucheng Zhou³

¹Nanjing Audit University, ²Xi'an University of Science and Technology

³SKL-IOTSC, CIS, University of Macau
yucheng.zhou@connect.um.edu.mo

Abstract

As automation advances in manufacturing, the demand for precise and sophisticated defect detection technologies grows. Existing vision models for defect recognition methods are insufficient for handling the complexities and variations of defects in contemporary manufacturing settings. These models especially struggle in scenarios involving limited or imbalanced defect data. In this work, we introduce MemoryMamba, a novel memory-augmented state space model (SSM), designed to overcome the limitations of existing defect recognition models. MemoryMamba integrates the state space model with the memory augmentation mechanism, enabling the system to maintain and retrieve essential defect-specific information in training. Its architecture is designed to capture dependencies and intricate defect characteristics, which are crucial for effective defect detection. In the experiments, MemoryMamba was evaluated across four industrial datasets with diverse defect types and complexities. The model consistently outperformed other methods, demonstrating its capability to adapt to various defect recognition scenarios.

1 Introduction

The advent of deep learning technologies has significantly advanced various industries [7, 32, 29, 6, 5], particularly manufacturing, by transforming defect recognition processes essential for quality control [41, 46]. In manufacturing, defect recognition plays a pivotal role in enhancing production efficiency, reducing costs, and ensuring product reliability. The demand for sophisticated and precise defect recognition systems has intensified as industries progress towards more automated and precise manufacturing techniques. These systems are essential not only for reducing the incidence of defective products reaching consumers but also for enhancing the overall sustainability of production lines through waste reduction and improved safety protocols.

The advent of Convolutional Neural Networks (CNNs) has significantly transformed defect recognition, enhancing both accuracy and automation [52, 64]. These models span from adaptations of established architectures like VGG [1] and ResNet [40] to more intricate configurations such as T-CNN [38] and GCNN [54], have significantly elevated the precision and speed of defect recognition systems [26]. The incorporation of techniques such as transfer learning and classifier fusion further enriches their adaptability and robustness across diverse manufacturing environments. Nevertheless, these models frequently encounter challenges in scenarios characterized by limited or highly imbalanced defect samples, i.e., conditions that are prevalent in specialized industrial settings. The dependency of these models on extensively annotated datasets to achieve high performance is a significant limitation, particularly in environments where such data is scarce.

State Space Models (SSMs) [21] have recently provided new avenues to address these challenges effectively. The Mamba model [19] and its variants in Computer Vision, such as VMamba [35]

and VIM [69], have demonstrated considerable potential in improving vision recognition. VMamba reduces computational complexity by leveraging the Cross-Scan Module (CSM), which performs 1D selective scanning in a 2D image space, thereby enabling global receptive fields without the heavy computational cost associated with Vision Transformers (ViTs). On the other hand, VIM employs bidirectional state space models along with position embeddings to handle image sequences, which helps in capturing comprehensive visual data necessary for identifying subtle and complex defects. Moreover, the efficiency and scalability of the Mamba model, due to its hardware-aware design, make it ideal for deployment in industrial settings where real-time processing is essential.

To address the above problems, we propose MemoryMamba, a novel memory-augmented state space model specifically designed for defect recognition tasks. The architecture of MemoryMamba combines state space techniques with memory augmentation to effectively capture dependencies and intricate defect characteristics. The model incorporates coarse- and fine-grained memory networks to better retain and access critical defect information from previously trained samples. Additionally, we introduce a fusion module that integrates features extracted from these memory networks, enhancing the model’s capability. Optimization strategies based on contrastive learning and mutual information maximization are also proposed for coarse- and fine-grained memory networks, respectively.

In the experiments, we evaluate the effectiveness of MemoryMamba by conducting comprehensive experiments across four industrial defect recognition datasets, encompassing a range of defect types and complexities. In addition, MemoryMamba consistently outperforms the existing models.

The main contributions of our paper are as follows:

- To the best of our knowledge, MemoryMamba is the first state space model for defect recognition in industrial applications.
- The MemoryMamba model incorporates a novel memory-augmented mechanism that allows for the retention and efficient retrieval of critical defect-related information from historical data.
- We design the optimization methods for coarse- and fine-grained memory networks, and propose a fusion module to integrate the visual feature and memory vector. Moreover, we propose optimization strategies, based on contrastive learning and mutual information maximization, for coarse-grained and fine-grained memory networks, respectively.
- Our experiments conducted a comprehensive comparative analysis with existing defect detection models, demonstrating MemoryMamba’s superior performance.

2 Related Work

2.1 Defect Recognition

With the advancement of deep learning applications across various industries [8, 33, 68, 67], defect detection technologies have become crucial in enhancing product quality and operational efficiency within the manufacturing industry, particularly with the emergence of Industry 4.0. These technologies integrate machine learning and computer vision, transforming traditional defect detection methods to achieve unprecedented accuracy and efficiency [2, 3, 11]. Significant advancements include the Tensor Convolutional Neural Network (T-CNN) developed by Martin-Ramiro et al. [38], which offers reduced parameter counts and improved training speeds without sacrificing accuracy. Similarly, Shi et al. [43] introduced the Center-based Transfer Feature Learning with Classifier Adaptation (CTFLCA), effectively adapting to diverse image distributions in different manufacturing settings and achieving high defect detection accuracies. Zaghoudi et al. [61] devise a classifier fusion approach for steel defect classification, combining SVM and RF with Bayesian rule, enhancing accuracy and speed. Moreover, there is an attempt to enhance the VGG19 into a Multipath VGG19, which improved defect detection across various datasets Apostolopoulos and Tzani [1]. In contrast, Fu et al. [14] effectively used a pretrained VGG16 model with a custom CNN classifier for detecting surface defects on steel strips, particularly in data-limited scenarios. In the area of X-ray imaging for quality control, Rafiei et al. [40] utilized a ResNet-based model optimized through structural pruning to enhance defect detection in mineral wool production. García Pérez et al. [18] developed Automated Defect Recognition (ADR) systems using CNNs that boost the reliability and speed of industrial X-ray analysis while minimizing subjective discrepancies. Gamdha et al. [15] develop

Sim-ADR, using synthetic data and ray tracing to train CNNs for X-ray anomaly detection with 87% accuracy. In addition, Gao et al. [16] proposed a method based on multilevel information fusion, ideal for small sample sizes, using a Gaussian pyramid with three VGG16 networks to enhance recognition accuracy. a subsequent work [17] involved a semi-supervised learning approach with CNNs enhanced by Pseudo-Label, leveraging both labeled and unlabeled data to improve defect detection.

Different from CNN-based methods, Wang et al. [54] introduced the Graph guided Convolutional Neural Network (GCNN), which incorporates a graph guidance mechanism into CNNs to enhance feature extraction and manage variations within defect classes. a subsequent work [50] introduced a deformable convolutional network (DC-Net) designed for mixed-type defect detection in wafer maps, achieving high accuracy with its novel structural design. Yu and Lu [59] present a manifold learning system with JLND for defect detection in wafer maps, outperforming traditional methods using WM-811K data. Specialized CNN adaptations for specific industrial applications include Tao et al. [47] for spring-wire sockets and Mentouri et al. [39] for online surface defect monitoring in the steel-making industry. Yang et al. [58] developed a model for detecting wind turbine blade damage, demonstrating superior performance in challenging environments. Other works in defect detection include the use of advanced neural network models by Konovalenko et al. [28] and Cheng and Yu [9] for rolled metal and steel surface defects. Su et al. [45] developed a Complementary Attention Network (CAN) within a faster R-CNN framework to refine defect detection in solar cell images. Zhang et al. [63] enhance DETR with ResNet, ECA-Net, dynamic anchors, and deformable attention for superior casting defect detection.

2.2 State Space Models

Different from Transformers [49, 65, 66, 30], State Space Models (SSMs) continue to evolve, increasingly shaping the frontier of sequence modeling by tackling the challenges of computational efficiency and long-range dependency management across various data types [53, 20, 62]. For time series forecasting, Xu et al. [57] introduced Mambaformer, a hybrid model combining Mamba and Transformer, efficiently managing both long and short-range dependencies and outperforming traditional models. Liang et al. [31] propose Bi-Mamba4TS, a model enhancing long-term forecasting with efficient computation and adaptive tokenization, outperforming current methods in accuracy. In computer vision, Chen and Ge [4] presented MambaUIE, optimizing state space models for Underwater Image Enhancement by efficiently combining global and local features, drastically reducing computational demands while maintaining high accuracy.

For image restoration, Deng and Gu [12] introduced the Channel-Aware U-Shaped Mamba (CU-Mamba) model, which incorporates a dual State Space Model into the U-Net architecture to efficiently encode global context and preserve channel correlations. In hyperspectral image denoising, Liu et al. [34] presented HSIDMamba, a Selective State Space Model that integrates advanced spatial-spectral mechanisms, significantly improving efficiency and performance, outperforming existing transformer-based methods by 30%. Moreover, Wang et al. [51] introduced InsectMamba, integrating State Space Models, CNNs, Multi-Head Self-Attention, and MLPs in Mix-SSM blocks to effectively extract detailed features for precise insect pest classification, demonstrating superior performance on various datasets. In the 3D point cloud analysis, Han et al. [22] developed Mamba3D, which leverages Local Norm Pooling and a bidirectional SSM, significantly surpassing Transformer models in both accuracy and scalability.

For medical imaging, several models demonstrate the application of SSMs: Wu et al. [55] proposed H-vmunet, enhancing feature extraction with High-order 2D-selective-scan (H-SS2D) and Local-SS2D modules. Yue and Li [60] introduced MedMamba, leveraging Conv-SSM modules to efficiently capture long-range dependencies. Ruan and Xiang [42] developed VM-UNet, using Visual State Space blocks for enhanced contextual information capture. Furthermore, Wu et al. [56] presented UltraLight VM-UNet, a highly efficient model using a novel PVM Layer for parallel feature processing.

In enhancing the capabilities of SSMs, He et al. [24] introduced DenseSSM, integrating shallow-layer hidden states into deeper layers to improve performance while maintaining efficiency. Smith et al. [44] introduced ConvS5, a convolutional state space model that excels in long spatiotemporal sequence modeling, training faster and generating samples more efficiently than competitors. Fathullah et al. [13] developed MH-SSM, a multi-head state space model that surpasses the transformer transducer on LibriSpeech and achieves state-of-the-art results when integrated into the Stateformer.

3 Preliminaries

3.1 State Space Models

State space models (SSMs) constitute a robust framework for the analysis of time series data, encapsulating the dynamics of systems through a series of mathematical representations. These models articulate the time series as a function of latent states and observations, with the state equations delineating the evolution of these latent states, and the observation equations describing the measurements derived from these states.

The evolution of the state vector \mathbf{x}_t at time t is governed by the state transition equation:

$$\mathbf{x}_t = \mathbf{F}_t \mathbf{x}_{t-1} + \mathbf{G}_t \mathbf{w}_t, \quad (1)$$

where \mathbf{F}_t denotes the state transition matrix that defines the dynamics of the state vector, \mathbf{G}_t represents the control-input matrix modulating the influence of the process noise, and \mathbf{w}_t is assumed to follow a Gaussian distribution with zero mean and covariance matrix \mathbf{Q}_t .

The observation model relates the observed data \mathbf{y}_t to the state vector through:

$$\mathbf{y}_t = \mathbf{H}_t \mathbf{x}_t + \mathbf{v}_t, \quad (2)$$

where \mathbf{H}_t is the observation matrix facilitating the mapping from the state space to the observed data, and \mathbf{v}_t is the observation noise, typically modeled as Gaussian with zero mean and covariance matrix \mathbf{R}_t .

The efficacy of state space models in capturing the dynamics of various systems hinges on the precise characterization of the matrices \mathbf{F}_t , \mathbf{G}_t , \mathbf{H}_t , and the noise processes \mathbf{Q}_t and \mathbf{R}_t . These matrices may be static or may vary with time, reflecting the changing dynamics of the system under study. The estimation of the latent states \mathbf{x}_t from the observations \mathbf{y}_t generally employs recursive algorithms such as the Kalman filter for linear models and particle filters for nonlinear variants. These methodologies rely on assumptions regarding the initial state distribution and the statistical properties of the noise components. This foundational description underscores the adaptability of state space models in addressing a myriad of applications across fields, where they are pivotal in modeling dynamic systems subjected to stochastic disturbances and observational noise.

4 MemoryMamba

In this section, we first elaborate on the overall architecture of MemoryMamba. Subsequently, we introduce our Mem-SSM Block, which includes our proposed Coarse- and Fine-Grained Memory Encoding and the Fusion Module.

4.1 Overall Architecture

Given an image \mathbf{I} with size of $H \times W \times 3$, the MemoryMamba model starts with the Patch Embedding procedure, as shown in Figure 1. The input image \mathbf{I} is transformed into embedded patch features \mathbf{F}_0 with dimensions of $\frac{H}{4} \times \frac{W}{4} \times C$, i.e.,

$$\mathbf{F}_0 = \text{PatchEmbed}(\mathbf{I}), \quad (3)$$

where $\mathbf{F}_0 \in \mathbb{R}^{\frac{H}{4} \times \frac{W}{4} \times C}$ denotes the embedded patch features. After the Patch Embedding, we employ the Mem-SSM Blocks to iteratively refine the feature representations, i.e.,

$$\mathbf{F}_i = \text{Mem-SSM-Block}(\mathbf{F}_{i-1}), \quad (4)$$

where \mathbf{F}_i and \mathbf{F}_{i-1} are the feature sets at the input and output of the i -th Mem-SSM Block, respectively. Our model consists of N Mem-SSM Blocks. Each block operation further compresses spatial dimensions and augments the channel capacity, effectively trading spatial granularity for feature depth. The final output \mathbf{F}_N is a high-dimensional representation that encapsulates the image’s semantic content.

The final output \mathbf{F}_N is then fed into a Multilayer perceptron (MLP) for classification, i.e.,

$$\mathbf{h} = \text{MLP}(\mathbf{F}_N), \quad (5)$$

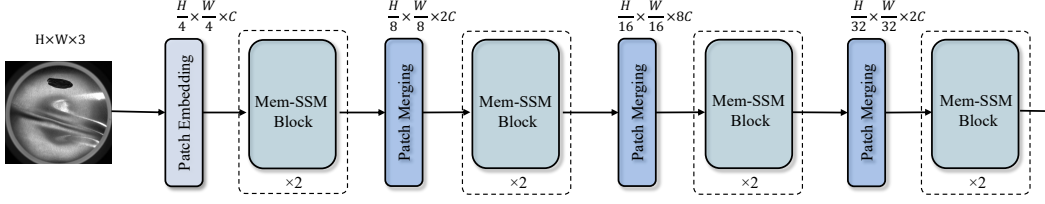


Figure 1: Overview of our method.

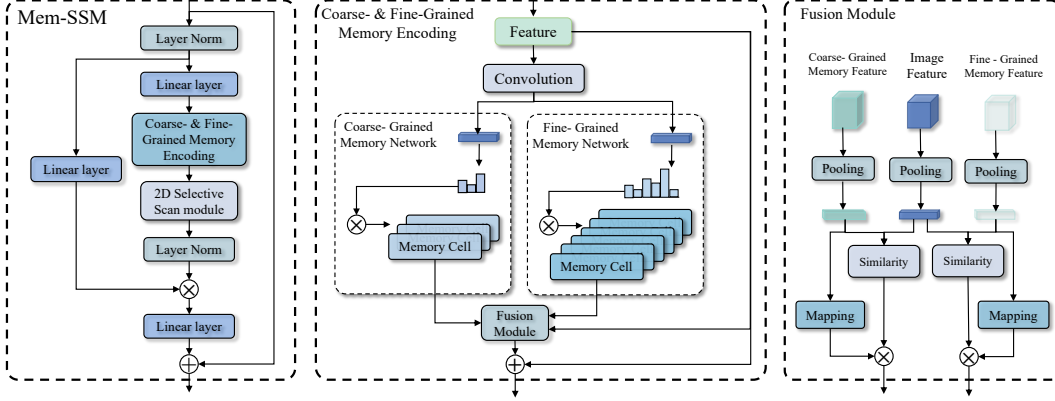


Figure 2: Details of Mem-SSM Block.

where \mathbf{h} denotes the hidden vector of the MLP. Then, we utilize the softmax function to compute the predicted probability distribution over the classes, i.e.,

$$\mathbf{p} = \text{softmax}(\mathbf{h}), \quad (6)$$

where $\mathbf{p} \in \mathbb{R}^K$ denotes the predicted probability distribution over K classes. Finally, our method can be trained end-to-end by minimizing the cross-entropy loss between the predicted probability distribution \mathbf{p} and the ground-truth label y , i.e.,

$$\mathcal{L}_{cls} = -\mathbf{y} \cdot \log(\mathbf{p}), \quad (7)$$

where \mathcal{L}_{cls} denotes the cross-entropy loss.

4.2 Mem-SSM Block

Due to the limited availability of defect samples, we design the Mem-SSM Block, which integrates memory networks to learn memory information from training samples. As shown in Figure 2, the Mem-SSM Block consists of memory encoding and selective scanning, thereby extracting a robust representation of the input that is particularly sensitive to the nuances required for accurate defect detection.

The block operates on the input features \mathbf{F}_{i-1} by initially passing them through a linear layer to produce an intermediate feature set \mathbf{Z}_i , which can be formally expressed as:

$$\mathbf{Z}_i = \text{Linear}(\mathbf{F}_{i-1}; \theta_{\text{Linear}}), \quad (8)$$

where θ_{Linear} represents the learnable parameters of the linear transformation.

Following the initial linear transformation, the Mem-SSM Block introduces the Coarse- and Fine-Grained Memory Encoding module, which is responsible for capturing and encoding hierarchical memory states. The memory encoding can be formulated as:

$$\mathbf{M}_i^{\text{coarse}}, \mathbf{M}_i^{\text{fine}} = \text{MemoryEncode}(\mathbf{Z}_i; \Theta_{\text{MemoryEncode}}), \quad (9)$$

where $\mathbf{M}_i^{\text{coarse}}$ and $\mathbf{M}_i^{\text{fine}}$ denote the coarse and fine memory states, respectively, and $\Theta_{\text{MemoryEncode}}$ denotes the set of parameters governing the memory encoding process.

To integrate these encoded memory states with the intermediate features, a fusion module is introduced:

$$\bar{\mathbf{F}}_i = \text{FusionModule}(\mathbf{M}_i^{\text{coarse}}, \mathbf{M}_i^{\text{fine}}, \mathbf{Z}_i; \Theta_{\text{Fusion}}), \quad (10)$$

where $\bar{\mathbf{F}}_i$ denotes the fused feature set and Θ_{Fusion} represents the parameters of the fusion module.

The fused features $\bar{\mathbf{F}}_i$ are then processed through the 2D Selective Scan module, which selectively emphasizes important feature responses while suppressing less relevant ones:

$$\mathbf{S}_i = \text{SelectiveScan}(\bar{\mathbf{F}}_i; \theta_{\text{SelectiveScan}}), \quad (11)$$

where \mathbf{S}_i is the selectively scanned feature set, and $\theta_{\text{SelectiveScan}}$ are the parameters of this module.

The output of the Selective Scan module is then normalized using a Layer Normalization step:

$$\mathbf{N}_i = \text{LayerNorm}(\mathbf{S}_i; \gamma, \beta), \quad (12)$$

where γ and β are the parameters for scaling and shifting during the normalization process.

The normalized features are combined with the original input features through a residual connection, followed by a second linear transformation:

$$\mathbf{F}_i = \text{Linear}(\mathbf{F}_{i-1} + \mathbf{N}_i; \theta'_{\text{Linear}}), \quad (13)$$

where θ'_{Linear} represents the learnable parameters of the second linear layer, which completes the processing within the Mem-SSM Block. The residual connection helps preserve the original feature information while allowing the network to learn modifications to the feature set adaptively.

By repeatedly applying the Mem-SSM Block, MemoryMamba progressively refines the visual representation.

4.2.1 Coarse- & Fine-Grained Memory Encoding

The Coarse- & Fine-Grained Memory Encoding is the crux of our Mem-SSM Block, as it underpins the model’s ability to discern and encode varying levels of feature details. This encoding mechanism is pivotal for nuanced tasks such as defect detection, where fine distinctions can determine the correct classification.

The memory encoding process begins with the application of a convolution operation to the intermediate feature set \mathbf{Z}_i , which serves to extract spatial hierarchies within the data:

$$\tilde{\mathbf{F}}_i = \text{Conv}(\mathbf{Z}_i; \theta_{\text{Conv}}), \quad (14)$$

where $\tilde{\mathbf{F}}_i$ is the convolution-processed feature set and θ_{Conv} denotes the convolutional layer’s parameters.

Upon obtaining $\tilde{\mathbf{F}}_i$, we proceed to map these features into memory vectors that embody the memory state at both coarse and fine levels. This mapping is achieved through a series of transformations that are designed to preserve the spatial correlations within the feature maps while reducing dimensionality to the desired memory size:

$$\begin{aligned} \mathbf{h}_c &= \text{MLP}_c(\tilde{\mathbf{F}}_i), \mathbf{h}_c \in \mathbb{R}^c, \\ \mathbf{h}_f &= \text{MLP}_f(\tilde{\mathbf{F}}_i), \mathbf{h}_f \in \mathbb{R}^f, \end{aligned} \quad (15)$$

where \mathbf{h}_c and \mathbf{h}_f represents the memory query vectors, and c and f are sizes of coarse- & fine-grained memory network.

Upon obtaining $\tilde{\mathbf{F}}_i$, we proceed to map these features into memory vectors that embody the memory state at both coarse and fine levels. This mapping is achieved through a series of transformations that are designed to preserve the spatial correlations within the feature maps while reducing dimensionality to the desired memory size:

$$\begin{aligned} \mathbf{h}_c &= \text{MLP}_c(\tilde{\mathbf{F}}_i), \mathbf{h}_c \in \mathbb{R}^c, \\ \mathbf{h}_f &= \text{MLP}_f(\tilde{\mathbf{F}}_i), \mathbf{h}_f \in \mathbb{R}^f, \end{aligned} \quad (16)$$

where \mathbf{h}_c and \mathbf{h}_f represents the memory query vectors, and c and f are sizes of coarse- & fine-grained memory network.

To assign relevance to these memory query vectors, a softmax layer is applied to generate a set of attention weights, thereby enabling the model to focus on the most pertinent memory vectors during the retrieval process:

$$\begin{aligned}\alpha_c &= \text{softmax}(\mathbf{h}_c) \\ \alpha_f &= \text{softmax}(\mathbf{h}_f)\end{aligned}\quad (17)$$

where α_c and α_f represent the attention weights for memory networks.

The final step in memory encoding involves the aggregation of memory knowledge by weighting the raw memory vectors with the attention weights, which is formalized as follows:

$$\begin{aligned}\bar{\mathbf{M}}_c &= \sum_j \alpha_j \cdot \mathbf{M}_{c,j}, \\ \bar{\mathbf{M}}_f &= \sum_t \alpha_t \cdot \mathbf{M}_{f,t},\end{aligned}\quad (18)$$

where $\bar{\mathbf{M}}_c$ and $\bar{\mathbf{M}}_f$ symbolize the aggregated memory vectors at both coarse and fine levels, and j and t index the individual memory vectors. The memory vectors $\bar{\mathbf{M}}_c$ and $\bar{\mathbf{M}}_f$ are subsequently made available to the Fusion Module, where they are fused with \mathbf{Z}_i .

4.2.2 Fusion Module

The Fusion Module is designed to merge the information from both the Coarse- and Fine-Grained Memory Encoding with the intermediate feature set \mathbf{Z}_i . The fusion process begins with the alignment of the memory vectors with the intermediate features, i.e.,

$$\begin{aligned}\mathbf{v}_c &= \text{Pooling}(\bar{\mathbf{M}}_c), \\ \mathbf{v}_f &= \text{Pooling}(\bar{\mathbf{M}}_f), \\ \mathbf{z}_i &= \text{Pooling}(\mathbf{Z}_i),\end{aligned}\quad (19)$$

$$\mathbf{z}_i = \text{Pooling}(\mathbf{Z}_i), \quad (20)$$

Then, we calculate the similarity between memory vectors and the feature:

$$\begin{aligned}\beta_c &= \text{Similarity}(\mathbf{v}_c, \mathbf{z}_i) \\ \beta_f &= \text{Similarity}(\mathbf{v}_f, \mathbf{z}_i)\end{aligned}\quad (21)$$

where β_c and β_f are the similarity scores between the coarse and fine memory vectors and the intermediate feature set respectively.

The similarity scores are used to modulate the contribution of the memory features. This is achieved through a weighting mechanism, which amplifies features that are relevant and suppresses the less significant ones:

$$\begin{aligned}\mathbf{w}_c &= \beta_c \cdot \mathbf{v}_c, \\ \mathbf{w}_f &= \beta_f \cdot \mathbf{v}_f,\end{aligned}\quad (22)$$

where \mathbf{w}_c and \mathbf{w}_f represent the weighted coarse and fine memory vectors. Then, we extend \mathbf{w}_c and \mathbf{w}_f to match the dimensionality of \mathbf{Z}_i . These expanded vectors are then added to \mathbf{Z}_i to form the enhanced feature set $\bar{\mathbf{F}}_i$.

4.3 Memory Network Optimization

To enhance the performance of the MemoryMamba architecture, specialized optimization strategies are employed for the Coarse-Grained and Fine-Grained Memory Networks. These strategies are designed to refine the memory encoding processes by leveraging both classification loss and unique memory-based losses.

4.3.1 Coarse-Grained Memory Network Optimization

The Coarse-Grained Memory Network is optimized using a contrastive learning approach, which leverages the query memory vectors \mathbf{h}_c from different classes. This method encourages the network to distinguish between the coarse features of various classes more effectively, i.e.,

$$\mathcal{L}_{\text{Contrastive}} = \sum_{k=1}^K \sum_{\substack{j=1 \\ j \neq k}}^K \max(0, \delta - \cos(\mathbf{h}_{c,k}, \mathbf{h}_{c,j})), \quad (23)$$

where $\mathbf{h}_{c,k}$ and $\mathbf{h}_{c,j}$ are the query memory vectors of the k -th and j -th class, respectively, \cos denotes the cosine similarity, and δ is a margin that defines the minimum acceptable distance between classes.

4.3.2 Fine-Grained Memory Network Optimization

For the Fine-Grained Memory Network, optimization is focused on maximizing the mutual information between the intermediate features \mathbf{Z}_i and their corresponding memory representations $\hat{\mathbf{M}}_f$, which have been processed through an MLP. The mutual information is maximized to ensure that the memory network captures detailed and relevant features that are crucial for fine-grained tasks, i.e.,

$$\mathcal{L}_{\text{NCE}} = -\mathbb{E}_{(\mathbf{Z}_i, \hat{\mathbf{M}}_f)} \left[\log \frac{e^{\text{sim}(\mathbf{Z}_i, \hat{\mathbf{M}}_f)}}{\sum_{\hat{\mathbf{M}}_f \in \mathcal{N}} e^{\text{sim}(\mathbf{Z}_i, \hat{\mathbf{M}}_f)}} \right], \quad (24)$$

where $\text{sim}(\cdot, \cdot)$ denotes a similarity metric (e.g., dot product), and \mathcal{N} represents a set of negative samples drawn from the memory that are not corresponding to \mathbf{Z}_i .

4.4 Overall Training Objective

The overall training objective combines the classification loss with the memory-specific losses to train the MemoryMamba model effectively:

$$\mathcal{L}_{\text{total}} = \mathcal{L}_{\text{cls}} + \lambda_c \mathcal{L}_{\text{contrastive}} + \lambda_f \mathcal{L}_{\text{NCE}}, \quad (25)$$

where λ_c and λ_f are weighting factors that balance the contribution of the contrastive and noise-contrastive estimation losses, respectively.

5 Experiments

5.1 Dataset

The Aluminum¹, GC10 [37], MT [25], and NEU [10] datasets are crucial for evaluating the performance of the defect recognition models. Each dataset includes a distinct number of categories and a split between training and testing data, as shown in Table 1. To assess model performance, we calculate the following metrics: Accuracy (ACC), Precision (Prec), Recall (Rec), and F1 Score. The comprehensive evaluation using these metrics allows us to thoroughly assess the performance of our defect recognition models, ensuring that they are robust and effective across different scenarios and dataset characteristics.

Table 1: Details of Defect Recognition Datasets.

Dataset	Category	Train	Test
Aluminum	4	277	123
GC10	10	1,834	458
MT	6	1,878	810
NEU	6	228	3,372

5.2 Experimental Setting

In this study, we utilized the Adam optimizer [27] to facilitate the learning process of our model. The learning rate is set to 2×10^{-5} , and the training process is 10 epochs. The weight decay was implemented at a rate of 0.01 to regularize and prevent the co-adaptation of neurons. Additionally, we incorporated a linear learning rate decay over the course of training, and a warm-up phase, accounting

¹<https://aistudio.baidu.com/datasetdetail/133083>

Table 2: Performance Comparison on Aluminum Dataset.

Method	ACC	Prec	Rec	F1
ResNet18	0.36	0.36	0.38	0.37
ResNet50	0.42	0.42	0.39	0.40
ResNet101	0.51	0.51	0.41	0.45
ResNet152	0.59	0.59	0.52	0.55
DeiT-S	0.36	0.36	0.28	0.32
DeiT-B	0.52	0.52	0.45	0.48
Swin-T	0.24	0.24	0.35	0.28
Swin-S	0.49	0.49	0.51	0.50
Swin-B	0.62	0.62	0.55	0.58
Vmamba-T	0.35	0.36	0.38	0.37
Vmamba-S	0.55	0.55	0.59	0.57
Vmamba-B	0.65	0.65	0.52	0.58
MemoryMamba	0.75	0.75	0.54	0.63

Table 3: Performance Comparison on GC10 Dataset.

Method	ACC	Prec	Rec	F1
ResNet18	0.55	0.55	0.53	0.48
ResNet50	0.71	0.71	0.67	0.67
ResNet101	0.74	0.74	0.68	0.66
ResNet152	0.77	0.77	0.73	0.71
DeiT-S	0.83	0.83	0.79	0.79
DeiT-B	0.84	0.84	0.82	0.82
Swin-T	0.71	0.71	0.75	0.70
Swin-S	0.79	0.79	0.70	0.70
Swin-B	0.86	0.86	0.78	0.79
Vmamba-T	0.79	0.79	0.80	0.78
Vmamba-S	0.83	0.83	0.78	0.79
Vmamba-B	0.83	0.83	0.84	0.82
MemoryMamba	0.90	0.90	0.89	0.89

Table 4: Performance Comparison on MT Dataset

Method	ACC	Prec	Rec	F1
ResNet18	0.69	0.69	0.56	0.55
ResNet50	0.83	0.83	0.71	0.72
ResNet101	0.86	0.86	0.77	0.79
ResNet152	0.88	0.88	0.73	0.78
DeiT-S	0.80	0.80	0.75	0.75
DeiT-B	0.84	0.84	0.77	0.78
Swin-T	0.82	0.82	0.62	0.67
Swin-S	0.83	0.83	0.71	0.74
Swin-B	0.88	0.88	0.76	0.80
Vmamba-T	0.87	0.87	0.89	0.86
Vmamba-S	0.91	0.91	0.91	0.90
Vmamba-B	0.92	0.92	0.87	0.89
MemoryMamba	0.96	0.96	0.97	0.96

Table 5: Model performance comparison on NEU Dataset.

Method	ACC	Prec	Rec	F1
ResNet18	0.86	0.86	0.78	0.72
ResNet50	0.89	0.86	0.89	0.87
ResNet101	0.94	0.94	0.93	0.93
ResNet152	0.94	0.94	0.94	0.94
DeiT-S	0.89	0.89	0.86	0.86
DeiT-B	0.93	0.93	0.91	0.91
Swin-T	0.88	0.87	0.88	0.88
Swin-S	0.91	0.91	0.85	0.84
Swin-B	0.92	0.92	0.92	0.92
Vmamba-T	0.91	0.92	0.89	0.90
Vmamba-S	0.92	0.91	0.91	0.91
Vmamba-B	0.94	0.94	0.94	0.94
MemoryMamba	0.99	0.99	0.99	0.99

for 5% of the total training duration, was also integrated. During this phase, the learning rate gradually increased from zero to the set initial rate. The batch size is set at 64 to optimize the model. Training is conducted using an NVIDIA 80 GB A100 GPU. The comparison methods include ResNet [23], DeiT [48], Swin-Transformer (Swin [36]), and Vmamba [35].

5.3 Results

Our experimental results across four datasets, i.e., Aluminum, GC10, MT, and NEU, demonstrate the superior performance of the MemoryMamba model. The comparison results are shown in Table 2, Table 3, Table 4, and Table 5. In comparison to traditional architectures like ResNet and transformer-based models such as DeiT and Swin Transformers, MemoryMamba consistently achieved the highest scores in Accuracy, Precision, Recall, and F1 Score. Notably, it outperformed in challenging defect detection scenarios, achieving as high as 99% in all evaluated metrics on the NEU dataset. The integration of Coarse- and Fine-Grained Memory Encoding significantly enhances the model’s ability to capture detailed contextual information, thus improving its effectiveness in complex visual pattern recognition tasks across diverse conditions.

5.4 Ablation Study

In the ablation study, we evaluate the contribution of the Coarse-Grained Memory Network (CMN), Fine-Grained Memory Network (FMN), and the Fusion Module within the MemoryMamba architecture. The removal of each component consistently led to a decrease in both accuracy and F1 scores, underscoring their individual and collective importance. The most significant performance drops occurred when multiple components were excluded simultaneously, highlighting their synergistic

Table 6: Ablation Study of MemoryMamba.

Method	Aluminum		GC10		MT		NEU	
	ACC	F1	ACC	F1	ACC	F1	ACC	F1
MemoryMamba	0.75	0.63	0.90	0.89	0.96	0.96	0.99	0.99
◇ w/o CMN	0.71	0.61	0.87	0.86	0.95	0.94	0.97	0.97
◇ w/o FMN	0.72	0.62	0.88	0.87	0.95	0.94	0.98	0.98
◇ w/o Fusion	0.72	0.61	0.88	0.88	0.95	0.94	0.97	0.98
◇ w/o CMN, Fusion	0.70	0.60	0.86	0.85	0.94	0.92	0.96	0.96
◇ w/o FMN, Fusion	0.70	0.60	0.87	0.85	0.94	0.93	0.96	0.96
◇ w/o CMN, FMN, Fusion	0.65	0.58	0.83	0.82	0.92	0.89	0.94	0.94



Figure 3: Comparison of similarity evaluation methods for Fusion Module on Aluminum (left) and GC10 (right) datasets.

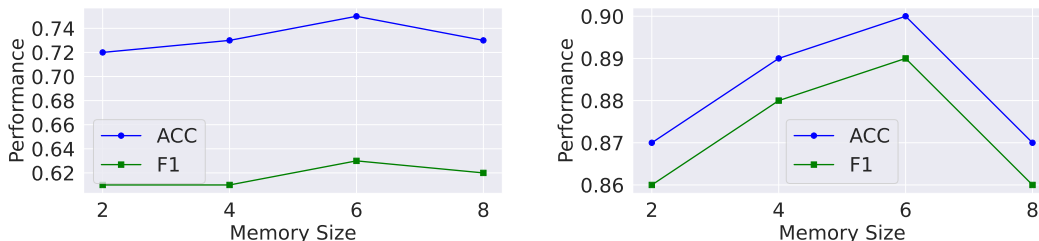


Figure 4: Investigation of different memory size for Coarse-grained Memory network on Aluminum (left) and GC10 (right) datasets.

effect. These findings emphasize the critical roles of CMN and FMN in capturing hierarchical feature details and the Fusion Module in effectively integrating these features, which are vital for the model’s performance and robustness in industrial defect detection tasks.

5.5 Impact on Fusion Module

The Fusion Module is critical to MemoryMamba, directly influencing its classification accuracy and F1 scores, as demonstrated in Figure 3. This module’s role in integrating Coarse- and Fine-Grained Memory Encodings with the feature set is validated through performance metrics on Aluminum and GC10 datasets using different similarity evaluation methods. Our findings highlight that Cosine similarity achieves higher performance on Aluminum and GC10. The choice of similarity metric thus plays a crucial role in tuning the Fusion Module for optimal defect detection performance.

5.6 Impact on Memory Networks

The performance of memory networks is crucial for the robustness of defect recognition systems. Our investigation, illustrated in Figures 4 and 5, highlights the influence of memory size on the accuracy (ACC) and F1 Score of Coarse-grained and Fine-grained Memory networks, respectively. For the Aluminum dataset, the Coarse-grained Memory network exhibits a peak performance at a memory size of 4, with diminishing returns as the size increases. On the more complex GC10 dataset,

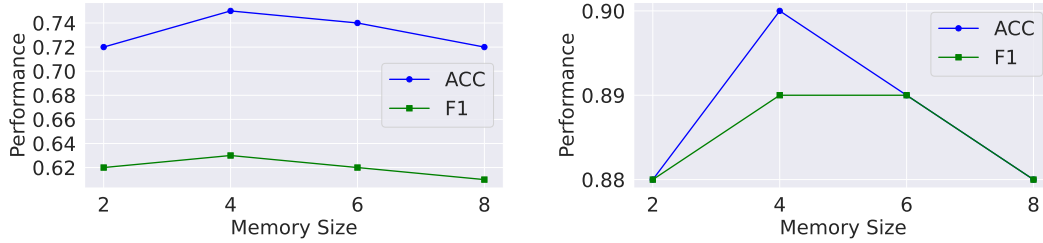


Figure 5: Investigation of different memory size for Fine-grained Memory network on Aluminum (left) and GC10 (right) datasets.

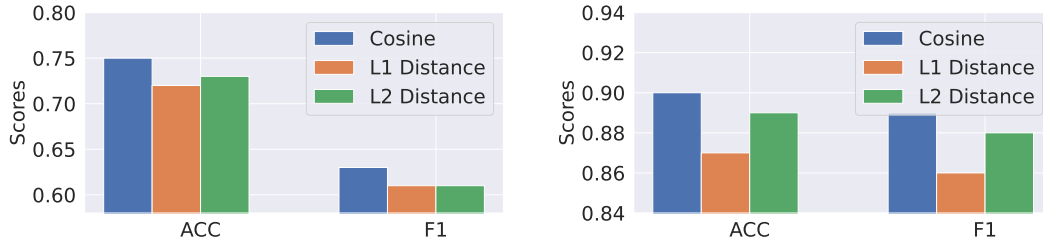


Figure 6: Impact of different similarity calculation methods for Coarse-grained Memory network on Aluminum (left) and GC10 (right) datasets.

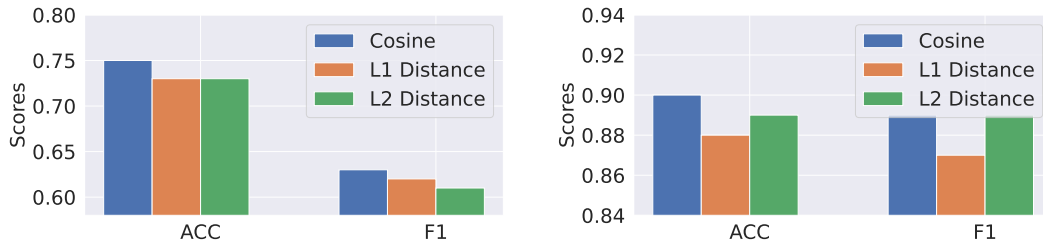


Figure 7: Impact of different similarity calculation methods for Fine-grained Memory network on Aluminum (left) and GC10 (right) datasets.

both memory network types show a significant performance variation with memory size changes. These observations suggest that the optimal memory size is contextually dependent on the dataset granularity and the network’s memory type.

5.7 Similarity Calculation on Memory Networks

For memory networks, the choice of similarity calculation method can significantly influence the performance of the model. To investigate this, we employed three different similarity measures: cosine similarity, L1 distance, and L2 distance, on coarse- and fine-grained memory networks. Figures 6 and 7 illustrate the impact of these methods on the Aluminum and GC10 datasets. Our observations reveal that cosine similarity consistently outperforms the L1 and L2 distances in the accuracy (ACC) and F1 score.

6 Conclusion

In this work, we integrate state space models with memory augmentation to address the limitations of other methods in defect recognition systems. We demonstrate that MemoryMamba’s unique architecture, which combines coarse-grained and fine-grained memory networks with a novel fusion module, effectively captures and utilizes historical defect-related data. This capability allows for enhanced detection of complex and subtle defects that previous models may overlook. The

application of contrastive learning and mutual information maximization strategies in optimizing these memory networks further enriches the robustness and accuracy of the defect detection process. The experimental results from four distinct industrial datasets have underscored MemoryMamba's superiority over existing technologies such as CNNs and Vision Transformers.

References

- [1] Ioannis D Apostolopoulos and Mpesiana Tzani. Industrial object, machine part and defect recognition towards fully automated industrial monitoring employing deep learning. the case of multilevel vgg19. *arXiv preprint arXiv:2011.11305*, 2020.
- [2] Prahar M Bhatt, Rishi K Malhan, Pradeep Rajendran, Brual C Shah, Shantanu Thakar, Yeo Jung Yoon, and Satyandra K Gupta. Image-based surface defect detection using deep learning: A review. *Journal of Computing and Information Science in Engineering*, 21(4):040801, 2021.
- [3] Yunkang Cao, Xiaohao Xu, Jiangning Zhang, Yuqi Cheng, Xiaonan Huang, Guansong Pang, and Weiming Shen. A survey on visual anomaly detection: Challenge, approach, and prospect. *arXiv preprint arXiv:2401.16402*, 2024.
- [4] Zhihao Chen and Yiyuan Ge. Mambaie&sr: Unraveling the ocean's secrets with only 2.8 flops, 2024.
- [5] Zhimin Chen, Longlong Jing, Yang Liang, YingLi Tian, and Bing Li. Multimodal semi-supervised learning for 3d objects. *arXiv preprint arXiv:2110.11601*, 2021.
- [6] Zhimin Chen, Longlong Jing, Liang Yang, Yingwei Li, and Bing Li. Class-level confidence based 3d semi-supervised learning. In *Proceedings of the IEEE/CVF Winter Conference on Applications of Computer Vision*, pages 633–642, 2023.
- [7] Zhimin Chen, Yingwei Li, Longlong Jing, Liang Yang, and Bing Li. Point cloud self-supervised learning via 3d to multi-view masked autoencoder. *arXiv preprint arXiv:2311.10887*, 2023.
- [8] Zhimin Chen, Longlong Jing, Yingwei Li, and Bing Li. Bridging the domain gap: Self-supervised 3d scene understanding with foundation models. *Advances in Neural Information Processing Systems*, 36, 2024.
- [9] Xun Cheng and Jianbo Yu. Retinonet with difference channel attention and adaptively spatial feature fusion for steel surface defect detection. *IEEE Transactions on Instrumentation and Measurement*, 70:1–11, 2020.
- [10] Ryan Cohn and Elizabeth Holm. Unsupervised machine learning via transfer learning and k-means clustering to classify materials image data. *Integrating Materials and Manufacturing Innovation*, 10:231–244, 2021. doi: 10.1007/s40192-021-00205-8.
- [11] Tamás Czimmermann, Gastone Ciuti, Mario Milazzo, Marcello Chiurazzi, Stefano Roccella, Calogero Maria Oddo, and Paolo Dario. Visual-based defect detection and classification approaches for industrial applications—a survey. *Sensors*, 20(5):1459, 2020.
- [12] Rui Deng and Tianpei Gu. Cu-mamba: Selective state space models with channel learning for image restoration, 2024.
- [13] Yassir Fathullah, Chunyang Wu, Yuan Shangguan, Junteng Jia, Wenhan Xiong, Jay Mahadeokar, Chunxi Liu, Yangyang Shi, Ozlem Kalinli, Mike Seltzer, and Mark J. F. Gales. Multi-head state space model for speech recognition, 2023.
- [14] Jingwen Fu, Xiaoyan Zhu, and Yingbin Li. Recognition of surface defects on steel sheet using transfer learning. *arXiv preprint arXiv:1909.03258*, 2019.
- [15] Dhruv Gamdha, Sreedhar Unnikrishnakurup, KJ Jyothis Rose, M Surekha, Padma Purushothaman, Bikash Ghose, and Krishnan Balasubramaniam. Automated defect recognition on x-ray radiographs of solid propellant using deep learning based on convolutional neural networks. *Journal of Nondestructive Evaluation*, 40(1):18, 2021.

- [16] Yiping Gao, Liang Gao, Xinyu Li, and Xi Vincent Wang. A multilevel information fusion-based deep learning method for vision-based defect recognition. *IEEE Transactions on Instrumentation and Measurement*, 69(7):3980–3991, 2019.
- [17] Yiping Gao, Liang Gao, Xinyu Li, and Xuguo Yan. A semi-supervised convolutional neural network-based method for steel surface defect recognition. *Robotics and Computer-Integrated Manufacturing*, 61:101825, 2020.
- [18] Alberto García Pérez, María José Gómez Silva, and A De La Escalera Hueso. Automated defect recognition of castings defects using neural networks. *Journal of nondestructive evaluation*, 41(1):11, 2022.
- [19] Albert Gu and Tri Dao. Mamba: Linear-time sequence modeling with selective state spaces. *arXiv preprint arXiv:2312.00752*, 2023.
- [20] Albert Gu, Karan Goel, and Christopher Ré. Efficiently modeling long sequences with structured state spaces. *arXiv preprint arXiv:2111.00396*, 2021.
- [21] James D Hamilton. State-space models. *Handbook of econometrics*, 4:3039–3080, 1994.
- [22] Xu Han, Yuan Tang, Zhaoxuan Wang, and Xianzhi Li. Mamba3d: Enhancing local features for 3d point cloud analysis via state space model, 2024.
- [23] Kaiming He, Xiangyu Zhang, Shaoqing Ren, and Jian Sun. Deep residual learning for image recognition. In *CVPR 2016, Las Vegas, NV, USA, June 27-30, 2016*, pages 770–778. IEEE Computer Society, 2016.
- [24] Wei He, Kai Han, Yehui Tang, Chengcheng Wang, Yujie Yang, Tianyu Guo, and Yunhe Wang. Densemamba: State space models with dense hidden connection for efficient large language models, 2024.
- [25] Yibin Huang, Congying Qiu, and Kui Yuan. Surface defect saliency of magnetic tile. *The Visual Computer*, 36(1):85–96, 2020.
- [26] Shashi Bhushan Jha and Radu F Babiceanu. Deep cnn-based visual defect detection: Survey of current literature. *Computers in Industry*, 148:103911, 2023.
- [27] Diederik P. Kingma and Jimmy Ba. Adam: A method for stochastic optimization. In *3rd International Conference on Learning Representations, ICLR 2015, San Diego, CA, USA, May 7-9, 2015, Conference Track Proceedings*, 2015.
- [28] Ihor Konovalenko, Pavlo Maruschak, Janette Brezinová, Ján Viňáš, and Jakub Brezina. Steel surface defect classification using deep residual neural network. *Metals*, 10(6):846, 2020.
- [29] Zhixin Lai, Jing Wu, Suiyao Chen, Yucheng Zhou, Anna Hovakimyan, and Naira Hovakimyan. Language models are free boosters for biomedical imaging tasks. *arXiv preprint arXiv:2403.17343*, 2024.
- [30] Zhixin Lai, Xuesheng Zhang, and Suiyao Chen. Adaptive ensembles of fine-tuned transformers for llm-generated text detection, 2024.
- [31] Aobo Liang, Xingguo Jiang, Yan Sun, and Chang Lu. Bi-mamba4ts: Bidirectional mamba for time series forecasting, 2024.
- [32] Tianrui Liu, Changxin Xu, Yuxin Qiao, Chufeng Jiang, and Weisheng Chen. News recommendation with attention mechanism. *arXiv preprint arXiv:2402.07422*, 2024.
- [33] Tianrui Liu, Changxin Xu, Yuxin Qiao, Chufeng Jiang, and Jiqiang Yu. Particle filter slam for vehicle localization. *arXiv preprint arXiv:2402.07429*, 2024.
- [34] Yang Liu, Jiahua Xiao, Yu Guo, Peilin Jiang, Haiwei Yang, and Fei Wang. Hsidmamba: Exploring bidirectional state-space models for hyperspectral denoising, 2024.
- [35] Yue Liu, Yunjie Tian, Yuzhong Zhao, Hongtian Yu, Lingxi Xie, Yaowei Wang, Qixiang Ye, and Yunfan Liu. Vmamba: Visual state space model. *arXiv preprint arXiv:2401.10166*, 2024.

- [36] Ze Liu, Yutong Lin, Yue Cao, Han Hu, Yixuan Wei, Zheng Zhang, Stephen Lin, and Baining Guo. Swin transformer: Hierarchical vision transformer using shifted windows. In *ICCV 2021, Montreal, QC, Canada, October 10-17, 2021*, pages 9992–10002. IEEE, 2021.
- [37] Xiaoming Lv, Fajie Duan, Jia-jia Jiang, Xiao Fu, and Lin Gan. Deep metallic surface defect detection: The new benchmark and detection network. *Sensors*, 20(6):1562, 2020.
- [38] Pablo Martin-Ramiro, Unai Sainz de la Maza, Roman Orus, and Samuel Mugel. Boosting defect detection in manufacturing using tensor convolutional neural networks, 2023.
- [39] Zoheir Mentouri, Hakim Doghmane, Abdelkrim Moussaoui, and Hocine Bourouba. Improved cross pattern approach for steel surface defect recognition. *The International Journal of Advanced Manufacturing Technology*, 110(11):3091–3100, 2020.
- [40] Mehdi Rafiei, Dat Thanh Tran, and Alexandros Iosifidis. Recognition of defective mineral wool using pruned resnet models. In *2023 IEEE 21st International Conference on Industrial Informatics (INDIN)*. IEEE, July 2023.
- [41] Zhonghe Ren, Fengzhou Fang, Ning Yan, and You Wu. State of the art in defect detection based on machine vision. *International Journal of Precision Engineering and Manufacturing-Green Technology*, 9(2):661–691, 2022.
- [42] Jiacheng Ruan and Suncheng Xiang. Vm-unet: Vision mamba unet for medical image segmentation, 2024.
- [43] Yan Shi, Lei Li, Jun Yang, Yixuan Wang, and Songhua Hao. Center-based transfer feature learning with classifier adaptation for surface defect recognition. *Mechanical Systems and Signal Processing*, 188:110001, 2023.
- [44] Jimmy T. H. Smith, Shalini De Mello, Jan Kautz, Scott W. Linderman, and Wonmin Byeon. Convolutional state space models for long-range spatiotemporal modeling, 2023.
- [45] Binyi Su, Haiyong Chen, Peng Chen, Guibin Bian, Kun Liu, and Weipeng Liu. Deep learning-based solar-cell manufacturing defect detection with complementary attention network. *IEEE Transactions on Industrial Informatics*, 17(6):4084–4095, 2020.
- [46] Jing Su, Chufeng Jiang, Xin Jin, Yuxin Qiao, Tingsong Xiao, Hongda Ma, Rong Wei, Zhi Jing, Jiajun Xu, and Junhong Lin. Large language models for forecasting and anomaly detection: A systematic literature review. *arXiv preprint arXiv:2402.10350*, 2024.
- [47] Xian Tao, Zihao Wang, Zhengtao Zhang, Dapeng Zhang, De Xu, Xinyi Gong, and Lei Zhang. Wire defect recognition of spring-wire socket using multitask convolutional neural networks. *IEEE Transactions on Components, Packaging and Manufacturing Technology*, 8(4):689–698, 2018.
- [48] Hugo Touvron, Matthieu Cord, Matthijs Douze, Francisco Massa, Alexandre Sablayrolles, and Hervé Jégou. Training data-efficient image transformers & distillation through attention. In *ICML 2021, 18-24 July 2021, Virtual Event*, volume 139 of *Proceedings of Machine Learning Research*, pages 10347–10357. PMLR, 2021.
- [49] Ashish Vaswani, Noam Shazeer, Niki Parmar, Jakob Uszkoreit, Llion Jones, Aidan N Gomez, Łukasz Kaiser, and Illia Polosukhin. Attention is all you need. *Advances in neural information processing systems*, 30, 2017.
- [50] Junliang Wang, Chuqiao Xu, Zhengliang Yang, Jie Zhang, and Xiaoou Li. Deformable convolutional networks for efficient mixed-type wafer defect pattern recognition. *IEEE Transactions on Semiconductor Manufacturing*, 33(4):587–596, 2020.
- [51] Qianning Wang, Chenglin Wang, Zhixin Lai, and Yucheng Zhou. Insectmamba: Insect pest classification with state space model. *arXiv preprint arXiv:2404.03611*, 2024.
- [52] Tian Wang, Yang Chen, Meina Qiao, and Hichem Snoussi. A fast and robust convolutional neural network-based defect detection model in product quality control. *The International Journal of Advanced Manufacturing Technology*, 94:3465–3471, 2018.

- [53] Xiao Wang, Shiao Wang, Yuhe Ding, Yuehang Li, Wentao Wu, Yao Rong, Weizhe Kong, Ju Huang, Shihao Li, Haoxiang Yang, et al. State space model for new-generation network alternative to transformers: A survey. *arXiv preprint arXiv:2404.09516*, 2024.
- [54] Yucheng Wang, Liang Gao, Yiping Gao, and Xinyu Li. A graph guided convolutional neural network for surface defect recognition. *IEEE Transactions on Automation Science and Engineering*, 19(3):1392–1404, 2022.
- [55] Renkai Wu, Yinghao Liu, Pengchen Liang, and Qing Chang. H-vmunet: High-order vision mamba unet for medical image segmentation, 2024.
- [56] Renkai Wu, Yinghao Liu, Pengchen Liang, and Qing Chang. Ultralight vm-unet: Parallel vision mamba significantly reduces parameters for skin lesion segmentation, 2024.
- [57] Xiongxiao Xu, Yueqing Liang, Baixiang Huang, Zhiling Lan, and Kai Shu. Integrating mamba and transformer for long-short range time series forecasting, 2024.
- [58] Xiyun Yang, Yanfeng Zhang, Wei Lv, and Dong Wang. Image recognition of wind turbine blade damage based on a deep learning model with transfer learning and an ensemble learning classifier. *Renewable Energy*, 163:386–397, 2021.
- [59] Jianbo Yu and Xiaolei Lu. Wafer map defect detection and recognition using joint local and nonlocal linear discriminant analysis. *IEEE Transactions on Semiconductor Manufacturing*, 29(1):33–43, 2015.
- [60] Yubiao Yue and Zhenzhang Li. Medmamba: Vision mamba for medical image classification, 2024.
- [61] Rachid Zaghoudi, Abdelmalek Bouguettaya, and Adel Boudiaf. Steel surface defect recognition using classifier combination. *The International Journal of Advanced Manufacturing Technology*, pages 1–17, 2024.
- [62] Hanwei Zhang, Ying Zhu, Dan Wang, Lijun Zhang, Tianxiang Chen, and Zi Ye. A survey on visual mamba, 2024.
- [63] Long Zhang, Sai-fei Yan, Jun Hong, Qian Xie, Fei Zhou, and Song-lin Ran. An improved defect recognition framework for casting based on detr algorithm. *Journal of Iron and Steel Research International*, 30(5):949–959, 2023.
- [64] Mei Zhang, Jinglan Wu, Huifeng Lin, Peng Yuan, and Yanan Song. The application of one-class classifier based on cnn in image defect detection. *Procedia computer science*, 114:341–348, 2017.
- [65] Yucheng Zhou and Guodong Long. Multimodal event transformer for image-guided story ending generation. In *Proceedings of the 17th Conference of the European Chapter of the Association for Computational Linguistics*, pages 3434–3444, 2023.
- [66] Yucheng Zhou and Guodong Long. Style-aware contrastive learning for multi-style image captioning. In *Findings of the Association for Computational Linguistics: EACL 2023*, pages 2257–2267, 2023.
- [67] Yucheng Zhou, Tao Shen, Xiubo Geng, Chongyang Tao, Can Xu, Guodong Long, Binxing Jiao, and Daxin Jiang. Towards robust ranker for text retrieval. In *Findings of the Association for Computational Linguistics: ACL 2023*, pages 5387–5401, 2023.
- [68] Yucheng Zhou, Tao Shen, Xiubo Geng, Chongyang Tao, Jianbing Shen, Guodong Long, Can Xu, and Daxin Jiang. Fine-grained distillation for long document retrieval. In *Proceedings of the AAAI Conference on Artificial Intelligence*, volume 38, pages 19732–19740, 2024.
- [69] Lianghai Zhu, Bencheng Liao, Qian Zhang, Xinlong Wang, Wenyu Liu, and Xinggang Wang. Vision mamba: Efficient visual representation learning with bidirectional state space model. *arXiv preprint arXiv:2401.09417*, 2024.